# Fabrication of Ag-Doped ZnO Photocatalysts Derived From MIL-125(Zn) With Enhanced Photocatalytic Activity

*Xiaobing Yang[1], Xiangrui Yang[2,3] and Shichao Wu[2,3]\**

[1]School of Photovoltaic Materials, Jiangxi New Energy Technology Institute, Xinyu, China, [2]Department of Nuclear Medicine, Xiangya Hospital, Central South University, Changsha, China, [3]National Clinical Research Center for Geriatric Disorders, Xiangya Hospital, Central South University, Changsha, China

Metal–organic frameworks (MOFs) have been widely used in various fields, including gas storage, separation, sensors, and catalysis, owing to their excellent performance. In this study, a zinc-based MOF [MIL-125(Zn)] was successfully synthesized using the solvothermal method, and Ag-doped ZnO (Ag/ZnO) was prepared by pyrolyzing Ag/MIL-125(Zn). The fabricated Ag/ZnO was used as a photocatalyst for rhodamine (RhB) degradation. Results showed that the MIL-125(Zn) derived from Ag/ZnO exhibits superior photocatalytic activity. It can degrade 99.4% of RhB under 20-min ultraviolet (UV) light irradiation, higher than those achieved using ZnO (73.2%) and MIL-125(Zn) (19.6%). Furthermore, Ag/ZnO shows excellent stability. After four photocatalytic degradation cycles, the photocatalytic activity of Ag/ZnO reduces by only 3.6%. The excellent photocatalytic performance of Ag/ZnO may be attributed to the synergistic effect of Ag nanoparticles and ZnO. The possible photocatalytic mechanism of RhB degradation on the Ag/ZnO photocatalyst under UV light irradiation was proposed.

Keywords: MIL-125(Zn), Ag/ZnO, RhB, degradation, photocatalytic activity

## INTRODUCTION

The wide usage of dyestuffs in various industries, such as textile, paper, rubber, and plastic, causes serious environmental problems because of the discharge of wastewater into water bodies (Pavithra et al., 2019). With increasing environmental protection awareness, the top priority is to determine an efficient approach for addressing the environmental problems associated with dyestuffs. Various chemical and physical methods are adopted to treat the wastewater containing dyestuffs, such as being adsorbed by porous carbon, adhered by chemical agents, and oxidized by ozone (Chang et al., 2013; Tabrizi et al., 2011; and Wang et al., 2021), but these methods are usually costly, inefficient, and prone to secondary contamination pollution (Sun et al., 2009). It is necessary to explore effective methods for treating dyestuff wastewater in a cost-effective and environmentally friendly manner.

Recently, semiconductor photocatalysis has been regarded as an innovative method of water treatment due to the ability of these semiconductors to degrade organic pollutants and toxic chemicals into nontoxic and harmful substances when exposed to UV and visible light irradiation. Until now, various semiconductors such as CdS (Prabha et al., 2018), CdWO$_4$ (Ye et al., 2008), TiO$_2$, and ZnO (Wang et al., 2011; Liu et al., 2019) have been explored. Among these semiconductor materials, ZnO has been widely used in various environmental remediation processes caused by

organic contaminants and microorganisms, owing to its excellent photocatalytic activity, nontoxicity, and stability features. In photocatalytic processes, the valence band can be inspired by photons to form holes ($h^+$), and the conduction band can receive photogenerated electrons ($e^-$). The photogenerated electron-hole pairs interact with the adsorbed $O_2$ and $OH^-$ on the catalyst surface to generate oxygen radicals ($O_2^-$) and hydroxyl radicals (OH). These photogenerated oxygen radicals ($O_2^-$) and hydroxyl radicals (OH) are produced *in situ*. They are highly reactive and unselective oxidants that can completely degrade organic pollutants (Subash et al., 2012). However, the photogenerated electron-hole pairs are easily recombined. It impedes the improvement of ZnO's photocatalytic activity. Researchers use various techniques to reduce the combination of photogenerated electron-hole pairs, such as doping with metals and combining with other materials. It is anticipated that inhibiting the combination of photogenerated electron-hole pairs will greatly improve ZnO's photocatalytic activity.

The zinc-based metal–organic framework [MIL-125(Zn)] is composed of $Zn^{2+}$ and organic ligands. Until now, there have been few reports on the fabrication of ZnO from MIL-125(Zn). In this study, MIL-125(Zn) was used as a precursor to prepare Ag-doped ZnO using absorption and pyrolysis processes, and the photocatalytic activity of the as-prepared Ag/ZnO was explored for RhB solution degradation under UV light irradiation. Results showed that MIL-125(Zn) can be completely transformed into ZnO, and Ag can be successfully doped in this MIL-125(Zn)-derived ZnO. The Ag/ZnO photocatalytic efficiency for RhB is up to 99.4%, which is far superior to that of ZnO (73.2%). Furthermore, Ag/ZnO exhibits excellent stability. The photocatalytic activity of Ag/ZnO was reduced only by 3.6% after four photocatalytic degradation cycles. The possible photocatalytic mechanism of RhB degradation on the Ag/ZnO photocatalyst under UV light irradiation is proposed. This work can provide experience for researchers who want to explore the use of MOFs in photocatalysis.

## EXOERUNEBTAL SECTUIB

## Fabrication of the Ag-Doped ZnO Photocatalyst

In this experiment, an Ag-doped ZnO photocatalyst was prepared using MIL-125(Zn) as a precursor. MIL-125(Zn) was synthesized with minor modifications following the previous report (Gao et al., 2020). First, 90 ml of DMF solution was mixed with 0.5 g of $H_2BDC$, 0.9 g of zinc nitrate hexahydrate, and 10 ml of methanol. The mixture was stirred for 30 min at room temperature. The mixture was then transferred into a teflon-lined stainless steel autoclave and heated at 150°C for 36 h. The synthesized precipitate was centrifuged, washed with DMF and ethanol thrice, and dried at 80°C to obtain MIL-125(Zn). Furthermore, 0.3 g of MIL-125(Zn) was dispersed in 3 ml of ethanol solution containing 0.3 ml of distilled water and 0.05 g of $AgNO_3$. The mixture was stirred for 30 min at room temperature. The mixture was then centrifuged and dried at 60°C for 24 h to obtain Ag/MIL-125(Zn). Finally, the obtained Ag/MIL-125(Zn) was placed in

a porcelain boat and heated to 550°C in a pipe furnace in an air atmosphere at a heating rate of 2°C/min to produce Ag-doped ZnO (Ag/ZnO). To make the comparisons, ZnO was also produced without doped Ag. The synthetic procedure for the Ag/ZnO photocatalyst is shown in **Figure 1**.

## Characterization

All samples' crystal phases were analyzed by X-ray diffraction (XRD) on a Bruker D8 diffractometer with Cu kα radiation (λ = 0.15406 nm) ranging from 5° to 80° (2θ). The morphology and internal structure analysis were carried out by scanning electron microscopy (SEM, JEOL Model 6500F) and transmission electron microscopy (TEM, JEOL JEM-2100). The Brunauer–Emmett–Teller (BET) specific surface area, pore-volume, and average pore diameter were calculated using $N_2$ adsorption/desorption isotherms obtained at −196°C using a Micromeritics APSP 2460 instrument. The UV-vis diffuse reflectance spectra (UV-vis DRS, UV-3600) in the wavelength range 200–800 nm were used to investigate the photoresponse performance of all samples. The Kubelka–Munk theory can be used to calculate the bandgap energy value (Mirzaeifard et al., 2020). The surface elemental composition and the chemical state of photocatalysts were determined by X-ray photoelectron spectroscopy (XPS; Thermo Scientific ESCALAB 250Xi).
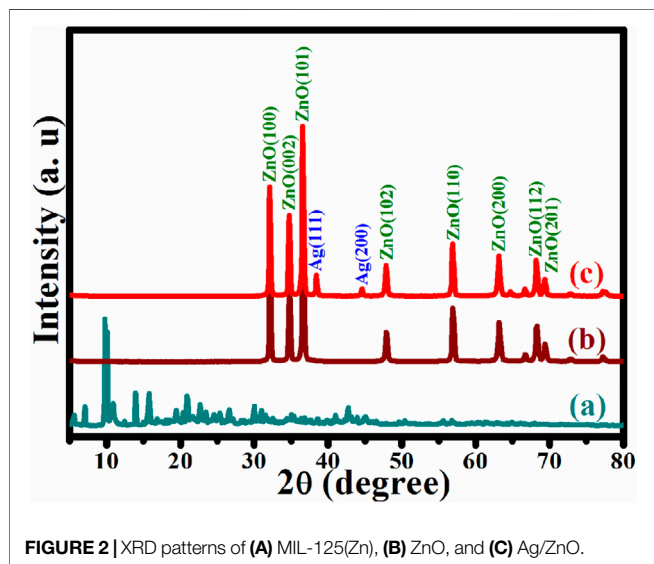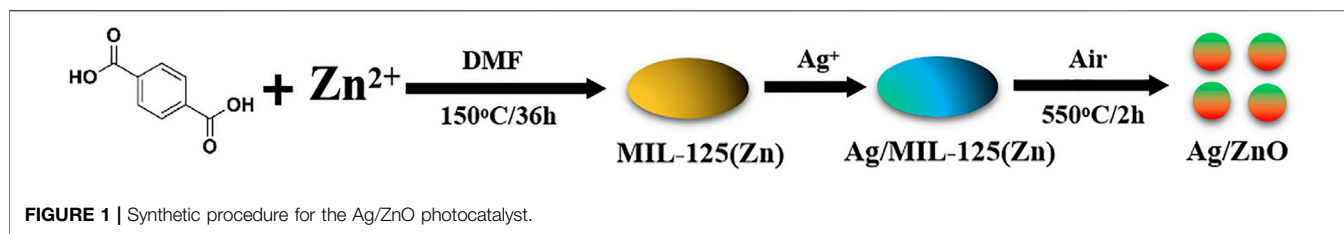
## Photocatalysis Experiments

The photocatalytic activity of all samples was evaluated using the degradation of RhB solution under UV light irradiation (300 W). In a cylindrical photoreactor, photocatalytic experiments were carried out. Furthermore, 0.05 g of the photocatalyst was well dispersed into 100 ml of the RhB solution for the typical photocatalytic measurement (5 ppm). To eliminate the influence of photocatalyst adsorption, the mixture was kept in the dark for 30 min to achieve the adsorption–desorption equilibrium. The mixture was then exposed to UV light, and 5 ml of it was extracted in 5-min interval. The extracted solution was centrifuged to remove the photocatalyst. A UV-vis spectrophotometer was used to examine the changes in the RhB concentration (UV-3600).

## RESULTS AND DISCUSSION

## X-Ray Diffraction Analysis

**Figure 2** shows the XRD patterns of MIL-125(Zn), ZnO, and Ag/ZnO. MIL-125(Zn) exhibits peaks at 5.62°, 7.03°, 9.75°, 10.85°, 13.89°, 15.76°, 19.42°, and 20.9° (**Figure 2A**), ascribed to the characteristic peaks of MIL-125(Zn), indicating its successful synthesis. When MIL-125(Zn) is treated at 550°C for 30 min at air temperature, eight obvious peaks appear at 31.13°, 34.78°, 36.57°, 47.87°, 56.91°, 63.15°, 68.21°, and 69.39° (**Figure 2B**), corresponding to the (100), (022), (101), (102), (110), (200), (112), and (201) reflections of ZnO, respectively (Hezam et al., 2017). **Figure 2C** shows the XRD patterns of Ag/ZnO and the characteristic peaks of ZnO. Moreover, it shows two new peaks at 38.44° and 44.60°, corresponding the (111) and (200) reflections of Ag, respectively (Yousefi and Hashemi,

**FIGURE 1 |** Synthetic procedure for the Ag/ZnO photocatalyst.



**FIGURE 2 |** XRD patterns of **(A)** MIL-125(Zn), **(B)** ZnO, and **(C)** Ag/ZnO.

2019). This confirms that Ag has been successfully doped in ZnO.

## SEM Analysis

The morphologies of MIL-125(Zn), ZnO, and Ag/ZnO were studied using the SEM technology (**Figure 3**). **Figure 3A** is the SEM image of MIL-125(Zn). The particle size of MIL-125(Zn) is approximately 200–500 nm. These nanoparticles have an obvious aggregation. **Figure 3B** shows the SEM image of ZnO. ZnO particles are smaller in size than MIL-125(Zn). This is attributed to the transformation of MIL-125(Zn)'s structure into ZnO. **Figure 3C** is the SEM image of Ag/ZnO. Ag/ZnO has a
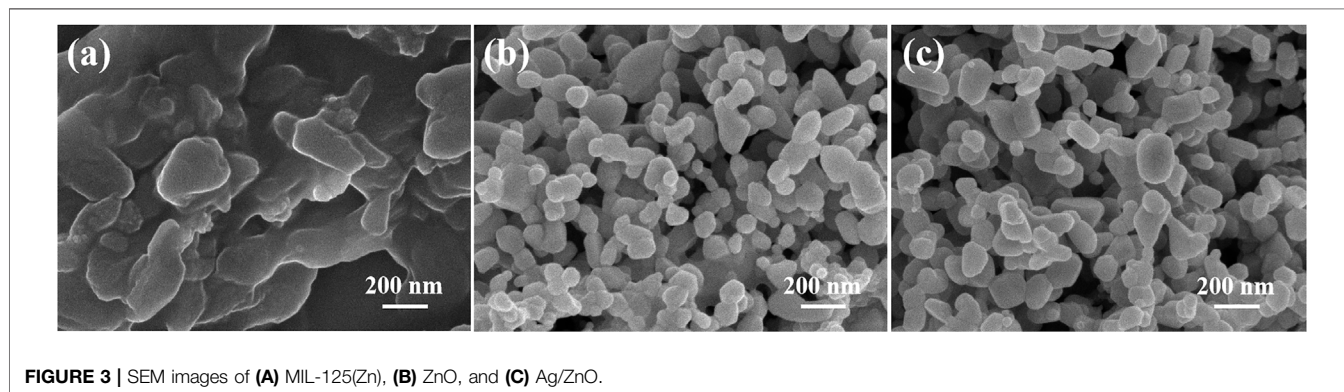
similar morphology to ZnO. Ag doping does not affect the morphology of ZnO.

## Brunauer–Emmett–Teller Analysis

**Figure 4** and **Table 1** show the $N_2$ adsorption–desorption isotherms and the textural parameters of MIL-125(Zn), ZnO, and Ag/ZnO. MIL-125(Zn) exhibits a type I curve, indicating the microporous structure, according to the IUPAC classification, as shown in **Figure 4A** (Zhang et al., 2018). **Figures 4B,C** show the $N_2$ adsorption–desorption isotherms of ZnO and Ag/ZnO, respectively. Both ZnO and Ag/ZnO exhibit the IUPAC type IV curve, indicating the mesoporous structure (Kruk and Jaroniec, 2001). The presence of mesoporous structures in ZnO and Ag/ZnO could be attributed to MIL-125(ZnO) decomposition and the release of volatile gases, such as $CO_2$ and $H_2O$ (Hu et al., 2020).

## UV-Vis Diffuse Reflectance Spectrum Analysis

The photoresponse performances of MIL-125(Zn), ZnO, and Ag/ZnO are investigated using UV-vis DRS. The bandgap energy can be calculated from the UV-DRS by $Eg = 1240/\lambda$ as abscissa and $(ah\nu)^2$. MIL-125(Zn) strongly absorbs UV light in the 200–300 nm wavelength range, as shown in **Figure 5A**. This is attributed to the characteristic absorption of MIL-125(Zn). When MIL-125(Zn) is heated, it exhibits a strong UV light absorption ability in the 200–400 nm wavelength range. MIL-125(Zn) is fully transformed into ZnO, according to the XRD patterns. This is attributed to ZnO's characteristic absorption ability. Surprisingly, Ag/ZnO exhibits a broad absorption in the visible light region compared to ZnO. The primary cause of this broad range of absorption is the energy transfer process from the conduction band to the metal ions (Pathak et al., 2018). The bandgap energy
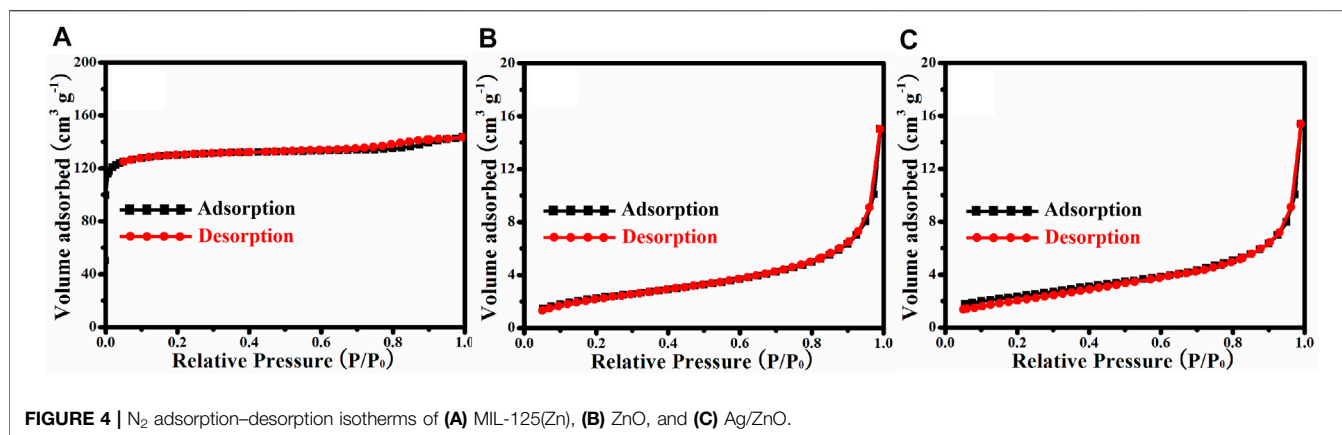


**FIGURE 3 |** SEM images of **(A)** MIL-125(Zn), **(B)** ZnO, and **(C)** Ag/ZnO.

**FIGURE 4 |** N$_2$ adsorption–desorption isotherms of **(A)** MIL-125(Zn), **(B)** ZnO, and **(C)** Ag/ZnO.

**TABLE 1 |** Textural parameters of MIL-125(Zn), ZnO, and Ag/ZnO.

| Sample | $S_{BET}$[a] | $S_{t-plot}$[b] | $V_{total}$[c] | $V_{micro}$[d] | D[e] |
|---|---|---|---|---|---|
| MIL-125(Zn) | 397.24 | 43.95 | 0.219 | 0.182 | 2.2 |
| ZnO | 9.15 | 8.38 | 0.012 | 0.024 | 5.9 |
| Ag/ZnO | 9.28 | 8.51 | 0.012 | 0.024 | 5.8 |

[a]Specific surface area (m$^2$/g).
[b]t-Plot external surface area.
[c]Total pore volume (cm$^3$/g).
[d]t-plot micropore volume (cm$^3$/g).
[e]Average pore diameter (nm).

value is a significant factor that affects the photocatalytic activity of the photocatalyst. **Figures 5B–D** show the bandgap energies of MIL-125(Zn), ZnO, and Ag/ZnO, which are 3.95, 3.26, and 3.24 eV, respectively. The lower bandgap energy value of Ag/ZnO appears to facilitate photon absorption easier than MIL-125(Zn) and ZnO, which may increase the photocatalytic activity when exposed to UV light.

## Transmission Electron Microscopy Analysis

The morphology and internal structure of Ag/ZnO were analyzed using low-magnification and high-magnification
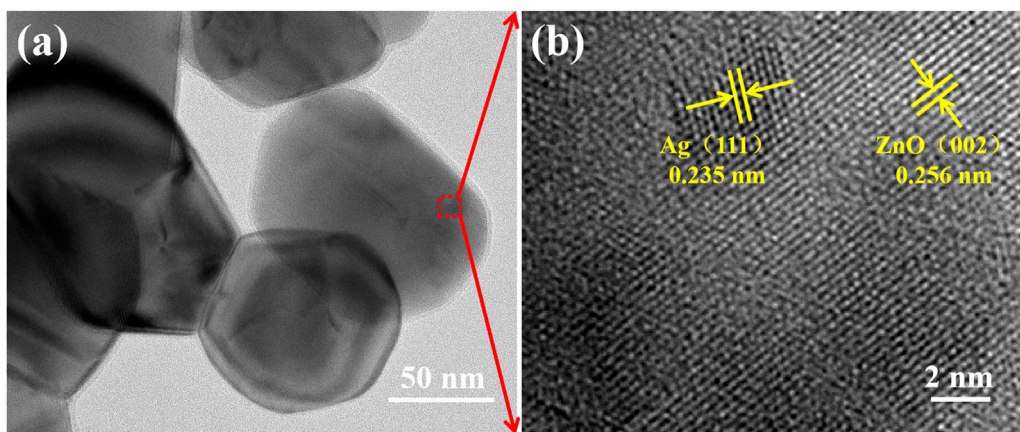


**FIGURE 5 |** **(A)** UV-vis diffuse reflectance spectra and **(B–D)** Kubelka–Munk plots of MIL-125(Zn), ZnO, and Ag/ZnO.
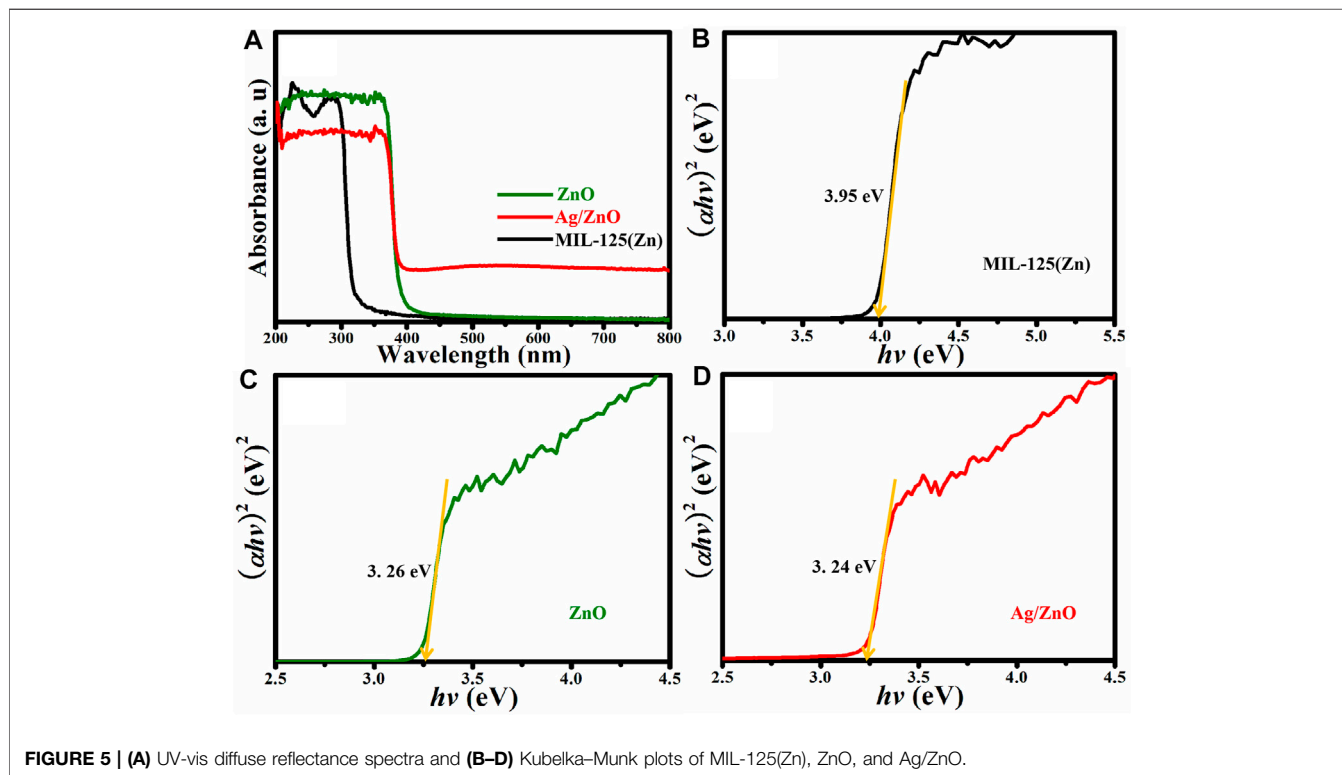
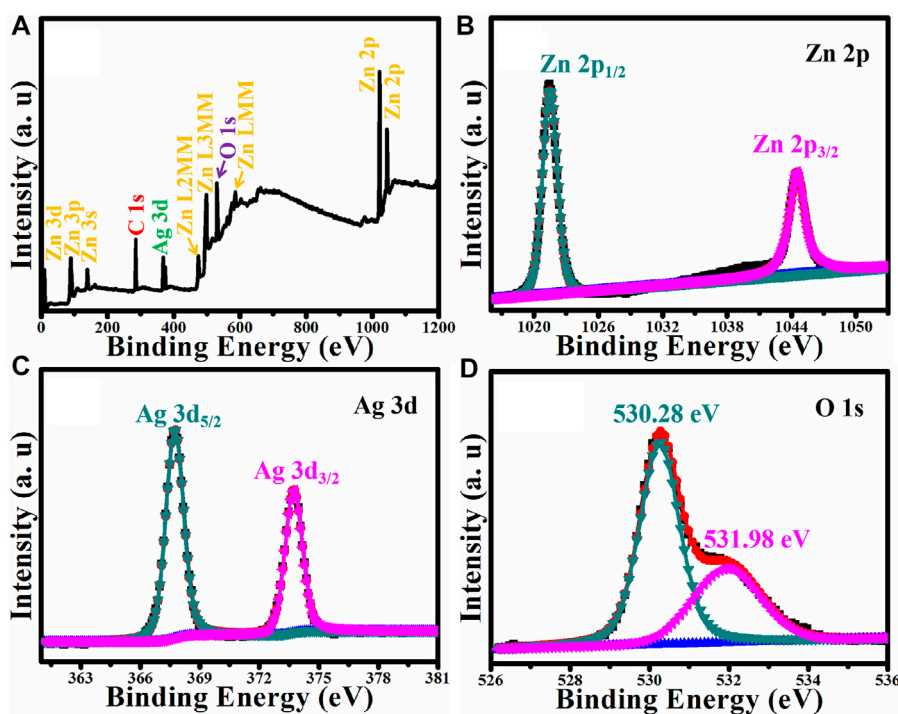**FIGURE 6 |** TEM image of Ag/ZnO: **(A)** low-magnification and **(B)** high-magnification.
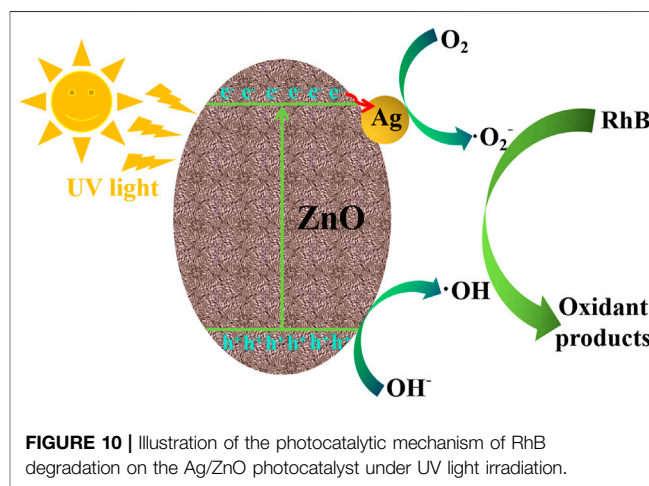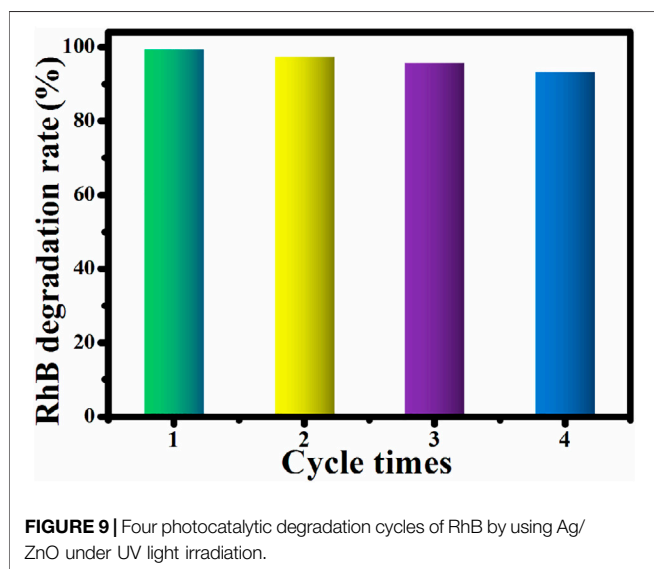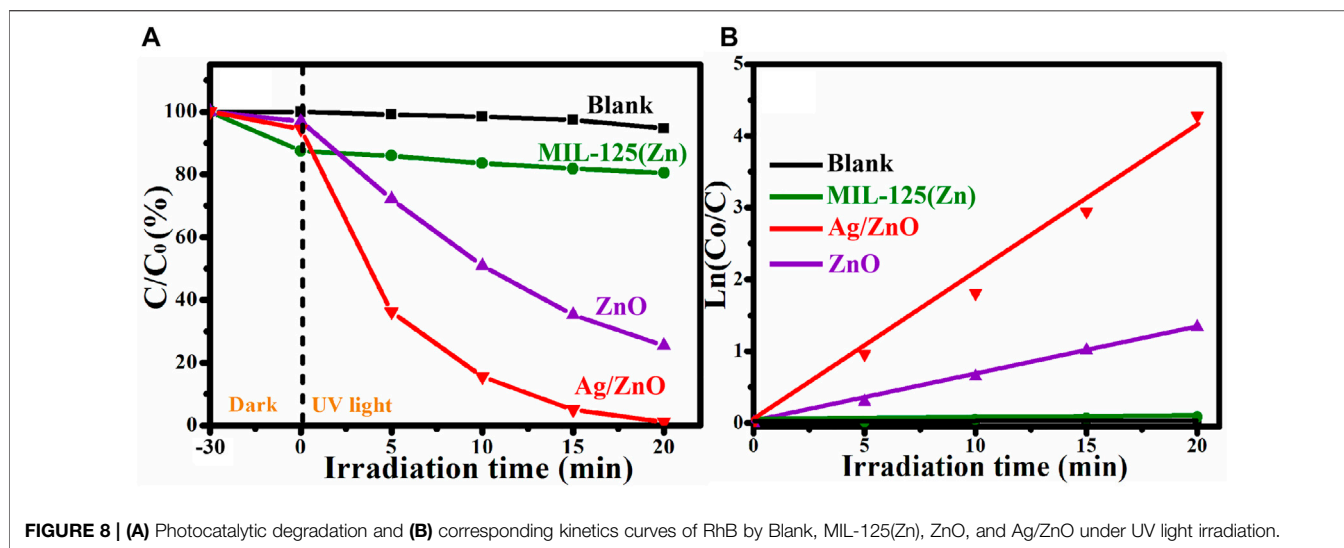


**FIGURE 7 | (A)** XPS survey spectrum of Ag/ZnO and the corresponding high resolution XPS spectra of **(B)** Zn 2p, **(C)** Ag 3d, and **(D)** O 1s.

TEM images. Ag/ZnO exhibits a nanoparticle morphology with particle sizes of ~100–200 nm (**Figure 6A**), consistent with the SEM results (**Figure 3B**). **Figure 6B** shows the high-magnification TEM image of Ag/ZnO, revealing distinct lattice fringes of 0.235 and 0.256 nm, corresponding to the (111) plane of Ag and the (002) plane of ZnO, respectively. This confirms that MIL-125(Zn) is fully transformed into ZnO, and Ag nanoparticles are well doped in MIL-125(Zn)-derived ZnO.

## X-Ray Photoelectron Spectroscopy Analysis

XPS was used to determine the surface elemental composition and the chemical state of Ag/ZnO. **Figure 7** shows the results. **Figure 7A** shows the XPS survey spectrum of Ag/ZnO. Ag/ZnO is made up of Ag, Zn, and O. The absorption of $CO_2$ produces the C signal. **Figure 7B** shows the Zn 2p spectrum, which is deconvoluted into two peaks at 1022.18 eV and 1045.28 eV, assigned to Zn $2p_{3/2}$ and Zn $2p_{1/2}$, respectively. The binding energy distance between Zn $2p_{1/2}$ and Zn

**FIGURE 8 | (A)** Photocatalytic degradation and **(B)** corresponding kinetics curves of RhB by Blank, MIL-125(Zn), ZnO, and Ag/ZnO under UV light irradiation.



**FIGURE 9 |** Four photocatalytic degradation cycles of RhB by using Ag/ZnO under UV light irradiation.



**FIGURE 10 |** Illustration of the photocatalytic mechanism of RhB degradation on the Ag/ZnO photocatalyst under UV light irradiation.

$2p_{3/2}$ is 23.1 eV, confirming ZnO's existence (Feng et al., 2020). **Figure 7C** shows the high-resolution XPS spectrum of Ag 3d, which shows two distinct peaks at 368.42 and 374.45 eV, which correspond to metallic silver ($Ag^0$) and silver ions ($Ag^+$), respectively (Zhao et al., 2020). **Figure 7D** shows the high-resolution O 1s spectrum. Deconvoluting O 1s yields two peaks at 530.28 and 531.98 eV, which can be assigned to Zn-O and C-O, respectively. Zn-O is assigned to ZnO, and C-O is assigned to absorb $CO_2$. The XPS analysis presented earlier confirms the successful fabrication of Ag-doped ZnO.
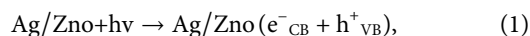
## Photocatalytic Degradation Properties

The degradation of RhB solution under UV light irradiation was used to investigate the photocatalytic activity of MIL-125(Zn), ZnO, and Ag/ZnO. To eliminate the influence of photocatalyst adsorption, all photocatalytic degradation experiments were carried out in the dark for 30 min before UV light irradiation. **Figure 8A** shows that after the 20-min UV light irradiation, Ag/ZnO can degrade 99.4% of RhB,

which is higher than ZnO (73.2%) and MIL-125(ZnO) (19.6%). Ag-doped ZnO can greatly improve the photocatalytic activity. **Figure 8B** shows the corresponding kinetics curves of RhB by Blank, MIL-125(Zn), ZnO, and Ag/ZnO under UV light irradiation. The photodegradation rate constant value of Ag/ZnO is approximately 0.25 $min^{-1}$, which is approximately 3.6 and 25 times greater than that of ZnO (0.07 $min^{-1}$) and MIL-125(Zn), respectively.

Aside from the photocatalytic activity, stability is critical for the photocatalyst. The photocatalyst Ag/ZnO was used to degrade the RhB solution for four photocatalytic degradation cycles under UV light irradiation, and the results are shown in **Figure 9**. During the photocatalytic degradation cycle experiment, the photocatalyst was centrifuged after each cycle experiment, washed thrice with distilled water, and dried at 80°C. **Figure 9** shows that after four photocatalytic degradation cycles, the photocatalytic activity of Ag/ZnO only decreases by 3.6%. Ag/ZnO exhibits excellent photocatalytic stability. The slight reduction of the photocatalytic efficiency may be caused by the unavoidable loss of Ag/ZnO during the cycle processes.

**Figure 10** shows the photocatalytic mechanism of RhB degradation on the Ag/ZnO photocatalyst under UV light irradiation. When exposed to UV light irradiation, electrons ($e^-$) in the valence band can absorb photons and transfer to the conduction band of ZnO, resulting in conduction band electrons ($e^-$) and valence band holes ($h^+$) (Sansenya et al., 2022). When ZnO is doped with Ag, the generated conduction band electrons ($e^-$) can more easily transform into Ag. This causes the electrons to accumulate on Ag nanoparticles and holes ($h^+$) to migrate to the surface of ZnO. It has the potential to greatly accelerate the separation of generated electrons ($e^-$) and holes ($h^+$). The generated electrons ($e^-$) and holes ($h^+$) can react with the adsorbed $O_2$ and $OH^-$ to form $O_2^-$ and OH, respectively, which are strong, oxidative species and can oxidize RhB molecular into nontoxic substances. The following are proposed photocatalytic reactions of RhB degradation on the Ag/ZnO photocatalyst:

$$Ag/Zno + hv \rightarrow Ag/Zno\left(e^-_{CB} + h^+_{VB}\right), \qquad (1)$$

$$e^-_{CB} + O_2 \rightarrow \cdot O_2^-, \qquad (2)$$

$$h^+_{VB} + OH^- \rightarrow \cdot OH, \qquad (3)$$

$$\cdot O_2^- + \cdot OH + RhB \rightarrow Oxidant\ products, \qquad (4)$$

## CONCLUSION

In conclusion, Ag/ZnO was successfully synthesized by pyrolyzing Ag/MIL-125(Zn) at high temperatures in an air atmosphere. Results

showed that doping Ag on MIL-125(Zn)-derived ZnO can broaden its UV light absorption ability to the visible light region, and Ag/ZnO shows improved photocatalytic activity for RhB degradation. Ag/ZnO achieves a higher degradation efficiency than ZnO (99.4% and 73.2%, respectively). The increased photocatalytic activity is attributed to Ag doping, which allows separation of photogenerated electrons and holes during recombination.

## DATA AVAILABILITY STATEMENT

The original contributions presented in the study are included in the article/supplementary material; further inquiries can be directed to the corresponding author.

## AUTHOR CONTRIBUTIONS

XY carried out the experiments and wrote the manuscript. XY carried out the experiments. SW designed the experiments.

## ACKNOWLEDGMENTS

## REFERENCES

Chang, B., Guan, D., Tian, Y., Yang, Z., and Dong, X. (2013). Convenient Synthesis of Porous Carbon Nanospheres with Tunable Pore Structure and Excellent Adsorption Capacity. *J. Hazard. Mater.* 262, 256–264. doi:10.1016/j.jhazmat.2013.08.054

Feng, C., Chen, Z., Jing, J., and Hou, J. (2020). The Photocatalytic Phenol Degradation Mechanism of Ag-Modified ZnO Nanorods. *J. Mat. Chem. C* 8, 3000–3009. doi:10.1039/c9tc05010h

Gao, Z., Wang, J., Muhammad, Y., Zhang, Y., Shah, S. J., Hu, Y., et al. (2020). Enhanced Moisture-Resistance and Excellent Photocatalytic Performance of Synchronous N/Zn-decorated MIL-125(Ti) for Vaporous Acetaldehyde Degradation. *Chem. Eng. J.* 388, 124389. doi:10.1016/j.cej.2020.124389

Hezam, A., Namratha, K., Drmosh, Q. A., Yamani, Z. H., and Byrappa, K. (2017). Synthesis of Heterostructured Bi2O3-CeO2-ZnO Photocatalyst with Enhanced Sunlight Photocatalytic Activity. *Ceram. Int.* 43, 5292–5301. doi:10.1016/j.ceramint.2017.01.059

Hu, C., Hu, X., Li, R., and Xing, Y. (2020). MOF Derived ZnO/C Nanocomposite with Enhanced Adsorption Capacity and Photocatalytic Performance under Sunlight. *J. Hazard. Mater.* 385, 121599. doi:10.1016/j.jhazmat.2019.121599

Kruk, M., and Jaroniec, M. (2001). Gas Adsorption Characterization of Ordered Organic–Inorganic Nanocomposite Materials. *Chem. Mat.* 13, 3169–3183. doi:10.1021/cm0101069

Liu, H., Li, D., Yang, X., and Li, H. (2019). Fabrication and Characterization of Ag3PO4/TiO2 Heterostructure with Improved Visible-Light Photocatalytic Activity for the Degradation of Methyl Orange and Sterilization of E.Coli. *Mater. Technol.* 34, 192–203. doi:10.1080/10667857.2018.1545391

Mirzaeifard, Z., Shariatinia, Z., Jourshabani, M., and Rezaei Darvishi, S. M. (2020). ZnO Photocatalyst Revisited: Effective Photocatalytic Degradation of Emerging Contaminants Using S-Doped ZnO Nanoparticles under Visible Light Radiation. *Ind. Eng. Chem. Res.* 59, 15894–15911. doi:10.1021/acs.iecr.0c03192

Pathak, T. K., Kroon, R. E., and Swart, H. C. (2018). Photocatalytic and Biological Applications of Ag and Au Doped ZnO Nanomaterial Synthesized by Combustion. *Vacuum* 157, 508–513. doi:10.1016/j.vacuum.2018.09.020

Pavithra, K. G., P., S. K., V., J., and P., S. R. (2019). Removal of Colorants from Wastewater: A Review on Sources and Treatment Strategies. *J. Industrial Eng. Chem.* 75, 1–19. doi:10.1016/j.jiec.2019.02.011

Prabha, D., Usharani, K., Ilangovan, S., Suganya, M., Balamurugan, S., Srivind, J., et al. (2018). Visible Light Irradiated Photocatalytic Activity of SnS2-CdS Nanocomposite against the Degradation of Methyl Orange Dye. *Mater. Technol.* 33, 333–339. doi:10.1080/10667857.2018.1444566

Sansenya, T., Masri, N., Chankhanittha, T., Senasu, T., Piriyanon, J., Mukdasai, S., et al. (2022). Hydrothermal Synthesis of ZnO Photocatalyst for Detoxification of Anionic Azo Dyes and Antibiotic. *J. Phys. Chem. Solids* 160, 110353. doi:10.1016/j.jpcs.2021.110353

Subash, B., Krishnakumar, B., Velmurugan, R., Swaminathan, M., and Shanthi, M. (2012). Synthesis of Ce Co-doped Ag-ZnO Photocatalyst with Excellent Performance for NBB Dye Degradation under Natural Sunlight Illumination. *Catal. Sci. Technol.* 2, 2319–2326. doi:10.1039/c2cy20254a

Sun, J.-H., Dong, S.-Y., Wang, Y.-K., and Sun, S.-P. (2009). Preparation and Photocatalytic Property of a Novel Dumbbell-Shaped ZnO Microcrystal Photocatalyst. *J. Hazard. Mater.* 172, 1520–1526. doi:10.1016/j.jhazmat.2009.08.022

Tabrizi, M. T. F., Glasser, D., and Hildebrandt, D. (2011). Wastewater Treatment of Reactive Dyestuffs by Ozonation in a Semi-batch Reactor. *Chem. Eng. J.* 166, 662–668. doi:10.1016/j.cej.2010.11.043

Wang, Y., Shi, R., Lin, J., and Zhu, Y. (2011). Enhancement of Photocurrent and Photocatalytic Activity of ZnO Hybridized with Graphite-like C3N4. *Energy Environ. Sci.* 4, 2922–2929. doi:10.1039/c0ee00825g

Wang, Z., Lü, S., Yang, F., Kabir, S. M. F., Mahmud, S., and Liu, H. (2021). Hyaluronate Macromolecules Reduced-Stabilized Colloidal Palladium Nanocatalyst for Azo Contaminated Wastewater Treatment. *Colloids*

*Surfaces A Physicochem. Eng. Aspects* 628, 127345. doi:10.1016/j.colsurfa.2021.127345

Ye, D., Li, D., Zhang, W., Sun, M., Hu, Y., Zhang, Y., et al. (2008). A New Photocatalyst CdWO4 Prepared with a Hydrothermal Method. *J. Phys. Chem. C* 112, 17351–17356. doi:10.1021/jp8059213

Yousefi, H. R., and Hashemi, B. (2019). Photocatalytic Properties of Ag@Ag-Doped ZnO Core-Shell Nanocomposite. *J. Photochem. Photobiol. A Chem.* 375, 71–76. doi:10.1016/j.jphotochem.2019.02.008

Zhang, B., Zhang, J., Tan, X., Shao, D., Shi, J., Zheng, L., et al. (2018). MIL-125-NH2@TiO2 Core-Shell Particles Produced by a Post-Solvothermal Route for High-Performance Photocatalytic H2 Production. *ACS Appl. Mat. Interfaces* 10, 16418–16423. doi:10.1021/acsami.8b01462

Zhao, S.-W., Zheng, M., Sun, H.-L., Li, S.-J., Pan, Q.-J., and Guo, Y.-R. (2020). Construction of Heterostructured G-C3N4/ZnO/cellulose and its Antibacterial Activity: Experimental and Theoretical Investigations. *Dalton Trans.* 49, 3723–3734. doi:10.1039/c9dt03757h